Comprehensive Analysis of mRNA Methylation Reveals Enrichment in 3′ UTRs and near Stop Codons

Kate D. Meyer,[1] Yogesh Saletore,[2,3] Paul Zumbo,[2,3] Olivier Elemento,[2,3] Christopher E. Mason,[2,3,*] and Samie R. Jaffrey[1,*]
[1]Department of Pharmacology
[2]Department of Physiology and Biophysics
[3]HRH Prince Alwaleed Bin Talal Bin Abdulaziz Alsaud Institute for Computational Biomedicine
Weill Medical College, Cornell University, New York, NY 10065, USA
*Correspondence: chm2042@med.cornell.edu (C.E.M.), srj2003@med.cornell.edu (S.R.J.)
DOI 10.1016/j.cell.2012.05.003

SUMMARY

Methylation of the N^6 position of adenosine (m^{6}A) is a posttranscriptional modification of RNA with poorly understood prevalence and physiological relevance. The recent discovery that FTO, an obesity risk gene, encodes an m^{6}A demethylase implicates m^{6}A as an important regulator of physiological processes. Here, we present a method for transcriptome-wide m^{6}A localization, which combines m^{6}A-specific methylated RNA immunoprecipitation with next-generation sequencing (MeRIP-Seq). We use this method to identify mRNAs of 7,676 mammalian genes that contain m^{6}A, indicating that m^{6}A is a common base modification of mRNA. The m^{6}A modification exhibits tissue-specific regulation and is markedly increased throughout brain development. We find that m^{6}A sites are enriched near stop codons and in 3′ UTRs, and we uncover an association between m^{6}A residues and microRNA-binding sites within 3′ UTRs. These findings provide a resource for identifying transcripts that are substrates for adenosine methylation and reveal insights into the epigenetic regulation of the mammalian transcriptome.

INTRODUCTION

The fat mass and obesity-associated (*FTO*) gene is a major regulator of metabolism and energy utilization (Church et al., 2009, 2010; Fischer et al., 2009). In humans, *FTO* polymorphisms that increase FTO expression are associated with elevated body mass index and increased risk for obesity (reviewed in Fawcett and Barroso, 2010). FTO is a member of the Fe(II)- and oxoglutarate-dependent AlkB oxygenase family and was originally shown to catalyze the oxidative demethylation of methylated thymidine and uracil (Gerken et al., 2007; Jia et al., 2008). However, FTO exhibits low activity toward these base modifica-

tions, and they are relatively infrequent with unclear physiological relevance (Klagsbrun, 1973). Thus, the physiologically relevant targets of FTO were unclear until recent studies that showed that FTO can demethylate N^6-methyladenosine (m^{6}A), a naturally occurring adenosine modification (Jia et al., 2011). These studies link adenosine methylation to physiological roles in human biological processes.

The distribution of m^{6}A in RNA is poorly understood. Previous studies have found that m^{6}A exists in RNA from a variety of unique organisms, including viruses, yeast, and mammals (Beemon and Keith, 1977; Bodi et al., 2010). m^{6}A is found in tRNA (Saneyoshi et al., 1969), rRNA (Iwanami and Brown, 1968), and viral RNA (Beemon and Keith, 1977; Dimock and Stoltzfus, 1977). Although m^{6}A is detectable in mRNA-enriched RNA fractions (Desrosiers et al., 1974), it has been confirmed in vivo in only one mammalian mRNA (Horowitz et al., 1984). The abundance of m^{6}A has been shown to be 0.1%–0.4% of total adenosine residues in cellular RNA (Dubin and Taylor, 1975; Perry et al., 1975; Wei et al., 1975), suggesting that this modification may be widespread throughout the transcriptome. Although the existence of m^{6}A has been known for many years, progress in establishing the prevalence of m^{6}A in mRNA has lagged behind that of other modified bases. This is due in large part to the lack of available methods for detecting the presence of m^{6}A. Because methylation of adenosine does not alter its ability to base pair with thymidine or uracil, m^{6}A is not amenable to detection with standard hybridization or sequencing-based methods.

Here, we examine the prevalence, regulation, and functional roles of m^{6}A in the transcriptome. We show that m^{6}A is a developmentally regulated RNA modification that is dynamically modified. Using antibodies that recognize m^{6}A, we have developed an affinity enrichment strategy that, when coupled with next-generation sequencing, allows for the high-throughput identification of m^{6}A sites. Using this approach, we present the first transcriptome-wide profile of m^{6}A localization in RNA. We find that m^{6}A is a widespread modification that is present in the mRNAs of >7,600 genes and in >300 noncoding RNAs. Additionally, m^{6}A is highly enriched near the stop codon and in the 3′ UTR. Furthermore, bioinformatic analysis of m^{6}A localization reveals consensus sites for m^{6}A and identifies a potential interaction between m^{6}A and microRNA pathways.
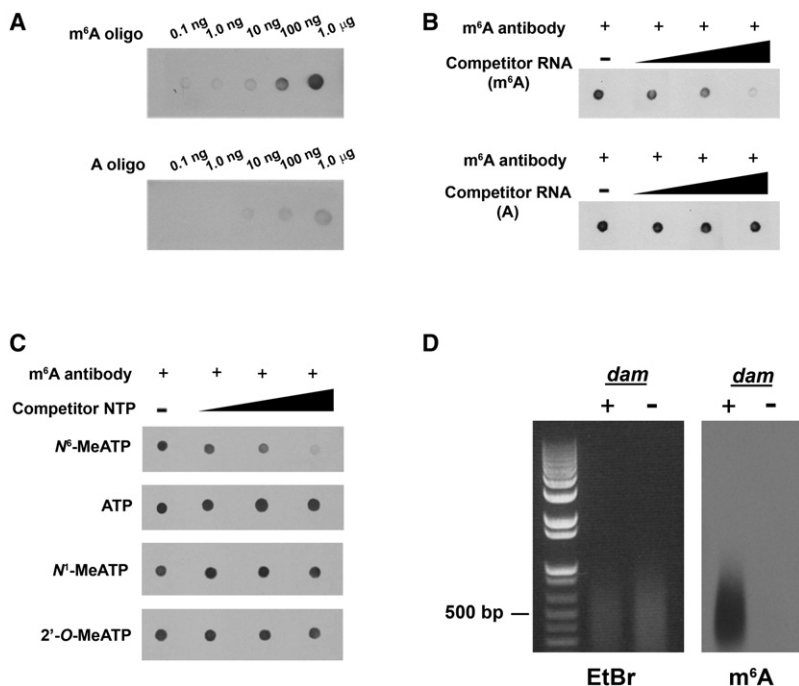
Figure 1. Specificity and Sensitivity of m⁶A-Specific Antibody

(A) Dot blot analysis demonstrates antibody specificity for m⁶A. Increasing amounts of an oligonucleotide containing either m⁶A or unmodified adenosine were spotted onto a membrane and probed with the m⁶A antibody. Though increased m⁶A immunoreactivity is observed in the presence of increasing concentrations of the m⁶A oligonucleotide (top), only background levels of immunoreactivity are observed at the highest concentrations of the A oligonucleotide (bottom). Blots shown are representative of results from three experiments.

(B) Competition dot blot assays were performed on membranes spotted with 100 ng of m⁶A-containing oligonucleotide. Antibody binding to the m⁶A oligonucleotide is attenuated by preincubation with increasing amounts of m⁶A-containing competitor RNA (top), but not with RNA containing unmodified adenosine (bottom). Amount of competitor RNA used (left to right): 0 ng (0 nM), 10 ng (0.1 nM), 100 ng (1.1 nM), 1 μg (11.2 nM). Blots shown are representative of results from four experiments.

(C) Competition dot blot assays were performed as in (B). Antibody was preincubated with increasing amounts of N⁶-methyladenosine triphosphate (N⁶-MeATP), adenosine triphosphate (ATP), N¹-methyladenosine triphosphate (N¹-MeATP), or 2′-O-methyladenosine triphosphate (2′-O-MeATP). Only N⁶-MeATP is able to compete with antibody binding. Concentration of competitor nucleotide used (left to right): 0 μM, 1 μM, 2 μM, 4 μM. Blots shown are representative of results from three experiments.

(D) Detection of m⁶A in cellular DNA. Genomic DNA isolated from *dam+* (containing m⁶A) or *dam−* (lacking m⁶A) *E. coli* was sheared and subjected to immunoblotting with the m⁶A antibody. Although 1.5 times as much DNA from *dam− E. coli* was loaded (left), the antibody only recognizes the m⁶A present in DNA from *dam+ E. coli* (right). Blot shown is representative of results from three experiments.

See also Figure S2.

RESULTS

Detection of m⁶A in Mammalian mRNA

Because m⁶A exhibits the same base pairing as unmodified adenosine, it is not readily detectable by standard sequencing or hybridization-based approaches. Additionally, m⁶A is not susceptible to chemical modifications that might otherwise facilitate its detection, such as bisulfite treatment, which is used to detect 5mC in DNA. The methods used thus far to detect m⁶A have involved treating cells with radiolabeled methionine, the precursor of the endogenous methylating agent *S*-adenosylmethionine, to impart radiolabeled methyl groups to adenosine (Csepany et al., 1990; Dubin and Taylor, 1975; Narayan and Rottman, 1988). Radiolabeled m⁶A residues are subsequently mapped with thin-layer chromatography or HPLC.

In order to simplify detection of m⁶A, we sought to develop an immunoblotting strategy. For these experiments, we used a previously described anti-m⁶A antibody (Bringmann and Lührmann, 1987; Jia et al., 2011; Munns et al., 1977). To ensure the specificity of this antibody for m⁶A, we performed dot blots using modified oligonucleotides immobilized to a membrane. The m⁶A antibody selectively bound to oligonucleotides containing a single m⁶A residue and exhibited negligible binding to oligonucleotides containing unmodified adenosine (Figure 1A). The binding was competed by incubating the antibody with increasing concentrations of an m⁶A-rich competitor RNA (Figure 1B). However, RNA containing unmodified adenosine did not compete for binding. Furthermore, binding was competed

by N⁶-methyladenosine triphosphate, but not by ATP or other modified adenosine triphosphates, including N¹-methyladenosine and 2′-O-methyladenosine (Figure 1C). Finally, to examine the specificity of the antibody in the context of other nucleotide sequences, we took advantage of the fact that the enzyme encoded by the *DNA adenine methylase* (*dam*) gene in *E. coli* methylates the N⁶ position of adenosine in DNA. Upon subjecting digested DNA isolated from *dam+* and *dam-* *E. coli* to immunoblotting using the m⁶A antibody, we found robust signals only in the DNA samples from the *dam+* strain (Figure 1D). Collectively, these data demonstrate the high sensitivity and selectivity of this antibody for m⁶A, as well as its ability to detect m⁶A within cellular nucleotide pools.

To explore the abundance of m⁶A within various RNA populations, we isolated RNA from several mouse tissues and subjected it to immunoblot analysis using the m⁶A antibody (Figure 2A). We found that m⁶A was present in all RNA samples tested, indicating that this modified nucleotide is widely distributed in many tissues, with particularly high enrichment in liver, kidney, and brain (Figure 2B). In addition, we observed large differences in the m⁶A content of various immortalized cell lines, including several cancer cell lines, which further indicates that large differences in m⁶A levels exist in different cell populations (Figure S1A available online).

m⁶A immunoreactivity was detected in bands throughout the molecular weight range of the blot (∼0.2 kb to ∼10 kb), consistent with incorporation of m⁶A in mRNA. Indeed, fractionation of whole cellular RNA into polyadenylated and nonpolyadenylated
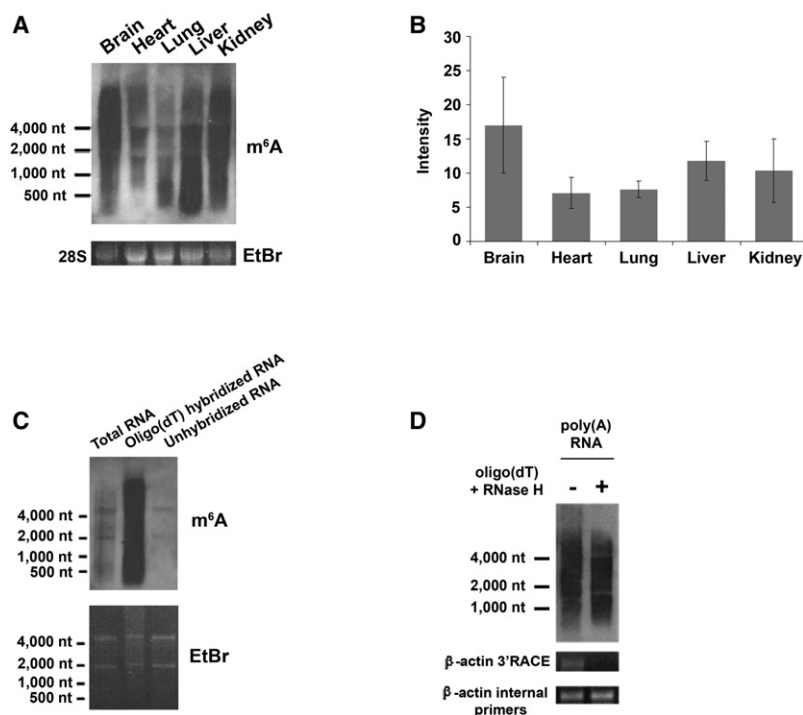
Figure 2. Distribution and Dynamic Cellular Regulation of m⁶A in RNA

(A) Widespread distribution of m^{6}A levels in a variety of tissues. Total RNA isolated from mouse brain, heart, lung, liver, and kidney (top) was subjected to m^{6}A immunoblot analysis. Ethidium bromide staining of the 28S rRNA is shown as a loading control (bottom).

(B) Quantification of m^{6}A abundance within various tissues. Quantification of m^{6}A immunoreactivity in (A) was measured by densitometry and normalized to the intensity of the corresponding 28S rRNA band for each tissue (n = 3; data are presented as mean ± SEM).

(C) m^{6}A is enriched within mRNAs. Oligo(dT) Dynabeads were used to isolate poly(A) RNA from total mouse brain RNA, and the unbound "flowthrough" RNA was saved as the poly(A)-depleted fraction. Equal amounts of total RNA, poly(A) RNA, and poly(A)-depleted RNA were then subjected to m^{6}A immunoblot analysis (top). Ethidium bromide staining of 28S rRNA is shown as a loading control (bottom). Intense m^{6}A immunoreactivity is observed in the poly(A) RNA fraction, consistent with high levels of m^{6}A within mRNAs.

(D) Depletion of poly(A) tails from mRNA does not reduce levels of m^{6}A in mRNA. Poly(A) RNA was isolated from total mouse brain RNA using oligo(dT) Dynabeads. Half of the sample was then subjected to poly(A) tail depletion by hybridizing to oligo(dT) primers and digestion with RNase H. Immunoblot analysis with the m^{6}A antibody (top) shows that levels of m^{6}A in poly(A) RNA (left) and poly(A) tail-depleted RNA (right) are comparable. Removal of poly(A) tails was confirmed using 3′RACE and RT-PCR to detect β-actin; no product is detected in the tail-depleted sample when oligo(dT) primers are used for cDNA synthesis (middle). As a control, use of random hexamers successfully generates a product in both samples (bottom).
See also Figure S1.

RNAs indicates that m^{6}A immunoreactivity is enriched in the polyadenylated RNA pool, which further suggests that m^{6}A in cellular RNA is localized to mature mRNA (Figure 2C). To determine whether m^{6}A is present in poly(A) tails, we selectively removed the poly(A) tail from cellular mRNA using oligo(dT) hybridization and RNase H treatment. Transcripts depleted of the poly(A) tail did not exhibit an appreciable reduction in m^{6}A levels (Figure 2D). In addition, immunoblotting poly(A) tails alone showed minimal m^{6}A immunoreactivity (Figures S2C–S2E). Together, these data demonstrate that m^{6}A is primarily an internal modification that is largely absent from the poly(A) tail.
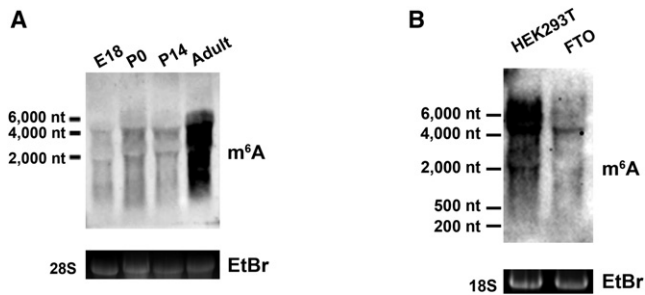
Dynamic Regulation of m⁶A

Our observation that m^{6}A is highly enriched within the brain prompted us to investigate the temporal dynamics of m^{6}A levels during different stages of neural development. Immunoblotting RNA samples with the m^{6}A antibody indicates that m^{6}A is present in mRNA at low levels throughout embryogenesis but increases dramatically by adulthood (Figure 3A). A similar increase in m^{6}A levels is also observed in RNA isolated from embryonic and postnatal rat brain cultured neurons (Figure S1B), which suggests that upregulation of m^{6}A levels accompanies neuronal maturation.

We next asked whether adenosine methylation is a dynamically regulated posttranscriptional modification and whether its levels can be regulated by specific demethylating enzymes. In our search for potential demethylating enzymes that act to remove the methyl group from m^{6}A, we focused on members of the family of Fe(II)- and 2-oxoglutarate-dependent oxygenases,

several of which have previously been shown to demethylate both DNA and RNA (Falnes et al., 2007; Gerken et al., 2007). Consistent with the findings of Jia et al. (2011), we observed that FTO decreased m^{6}A levels when overexpressed in mammalian cells (Figure 3B). Furthermore, we find that overexpression of FTO resulted in a broad size range of RNAs that exhibit reduced m^{6}A immunoreactivity (Figure 3B).

MeRIP-Seq Identifies m⁶A-Containing RNAs throughout the Transcriptome

In order to obtain insight into potential roles for m^{6}A, we sought to characterize its distribution throughout the transcriptome. To do this, we first determined whether the m^{6}A antibody could be used to enrich m^{6}A-containing RNAs. In vitro immunoprecipitation experiments showed that a single round of MeRIP produces ∼70-fold enrichment, and two rounds produce >130-fold enrichment for m^{6}A-containing targets (Figure S3). To identify m^{6}A sites throughout the transcriptome, we developed a method that combines m^{6}A-specific methylated RNA immunoprecipitation (MeRIP) with next-generation sequencing (RNA-Seq). The procedure for MeRIP-Seq (outlined in Figure 4A) involves randomly fragmenting the RNA to ∼100 nt sized fragments prior to immunoprecipitation. Because an m^{6}A site could lie anywhere along the length of a given immunoprecipitated 100 nt fragment, sequencing reads are expected to map to a region that contains the m^{6}A site near its center. At its extremes, this region would be predicted to be roughly 200 nt wide (100 nt up- and downstream from the m^{6}A site) (Figures 4B and 4C).

A

6,000 nt
4,000 nt
2,000 nt

m⁶A

E18 P0 P14 Adult

28S   EtBr

B

6,000 nt
4,000 nt
2,000 nt
500 nt
200 nt

m⁶A

HEK293T FTO

18S   EtBr

Figure 3. Regulation of m^{6}A Levels in Cells and during Development
(A) Ontogeny of m^{6}A abundance throughout brain development. Total RNA was isolated from mouse brain at embryonic day 18 (E18), postnatal day 0 (P0), postnatal day 14 (P14), and adulthood and was then subjected to immunoblot analysis to detect m^{6}A-containing transcripts. Ethidium bromide staining of 28S rRNA bands is shown as a loading control.
(B) FTO demethylates a wide range of cellular transcripts. FTO was expressed in HEK293T cells for 48 hr, and cellular RNA was subjected to immunoblot analysis to detect m^{6}A.
See also Figure S1.

We next utilized MeRIP-Seq to identify m^{6}A sites in total mouse brain RNA. Reads from the MeRIP sample frequently mapped to mRNAs and clustered as distinct peaks. As predicted, these peaks frequently converged to ~100 nt wide regions near their midpoint (Figure 4C). Furthermore, enrichment of reads in these regions was not observed in the non-IP control sample, which was composed of the input RNA prior to m^{6}A immunoprecipitation, demonstrating the specificity of these peaks (Figure S3).

To determine the location of these peaks throughout the transcriptome and thus characterize the regions of m^{6}A localization, we developed an algorithm for identifying m^{6}A peaks (see Extended Experimental Procedures). Additionally, we performed replicate MeRIP-Seq experiments in which we utilized: (1) a different sequencing platform (Illumina's GAIIx versus HiSeq2000), (2) independently prepared RNA samples from different animals, and (3) an unrelated m^{6}A antibody (Kong et al., 2000), which exhibited similarly high specificity for m^{6}A (Figure S4). We employed our algorithm to identify m^{6}A peaks that met a minimum p value (p ≤ 0.05, Benjamini and Hochberg corrected) within each individual sample. From the three samples, we identified a total of 41,072 distinct peaks in the RNAs of 8,843 genes, which we call our "filtered" set of m^{6}A peaks (Table S1). Of these peaks, 80% were detected in at least two different replicates. The high concordance between these samples indicates that MeRIP-Seq is highly reproducible across different sequencing platforms and using different m^{6}A antibodies. For subsequent bioinformatic analyses, we used the list of 13,471 m^{6}A peaks in RNAs from 4,654 genes that were detected in all three replicates (our "high-confidence" list; Table S2A). This list demonstrates the presence of m^{6}A in a substantial fraction of the transcriptome and indicates that m^{6}A is a common feature of mammalian mRNAs.

m^{6}A Is Detected in Noncoding RNAs

The majority of our high-confidence m^{6}A peaks (94.5%) are found within mRNAs. However, we also observed that 236

(1.8%) of our peaks mapped to noncoding RNAs (ncRNAs) that were annotated in the RefSeq database (Table S2A). In addition, 588 m^{6}A peaks did not map to a known RefSeq mRNA or ncRNA. To determine whether these unannotated peaks localize to ncRNAs predicted in other databases, we aligned them to genomic regions of a set of 32,211 ncRNAs from the RIKEN functional annotation of mouse (FANTOM3) data set that we obtained from the mammalian noncoding RNA database (RNAdb; Pang et al., 2005). We found that 216 of these peaks mapped to a FANTOM3 ncRNA (Table S2B). All of these ncRNAs were >200 nt in length, indicating that long ncRNAs are substrates for adenosine methylation. Additionally, when we interrogated a set of conserved human lincRNAs (Cabili et al., 2011) for overlaps with m^{6}A peaks, we found nine additional peaks that overlapped with these lincRNAs (Table S2C). Collectively, these data identify several classes of ncRNAs as targets of adenosine methylation.

### Biochemical Validation of m^{6}A-Containing Transcripts

We next sought to validate the presence of m^{6}A in mRNAs identified with MeRIP-Seq. To do this, we used RNA pull-down assays to isolate individual mRNAs from total mouse brain RNA by hybridization to target-specific probes. Isolated mRNAs were then subjected to immunoblot analysis using the m^{6}A antibody to detect the presence of m^{6}A. Using this method, we validated the presence of m^{6}A within *low density lipoprotein receptor* (*Ldlr*) (Figures 5A and 5B), *metabotropic glutamate receptor 1* (*Grm1*), and *dopamine receptor D1A* (*Drd1a*) (Figures S5A–S5D). These mRNAs were chosen to demonstrate our ability to validate m^{6}A presence in transcripts with multiple methylation sites (*Grm1* and *Drd1a*) as well as those with single m^{6}A peaks (*Ldlr*). To further demonstrate that MeRIP-Seq selectively enriches for these endogenous methylated targets, we performed qRT-PCR on the unbound fractions after RNA precipitation with the m^{6}A antibody. As expected, we observed substantial immunodepletion of *Grm1*, *Drd1a*, and other methylated targets in the unbound fraction. In contrast, transcripts that lack m^{6}A peaks, such as *Rps21* and *Ndel1*, were detectable at high levels in the unbound fraction (Figure S5E).

m^{6}A-Containing mRNAs Are Involved in Important Biological Pathways

To predict potential signaling pathways and cellular processes that involve m^{6}A, we used the DAVID bioinformatics database to identify the gene ontology (GO) terms that are enriched for m^{6}A-containing transcripts. We found that genes encoding m^{6}A-containing RNAs are involved in a variety of cellular functions, including transcriptional regulation, RNA metabolism, and intracellular signaling cascades (Table S5). In addition, we observed that m^{6}A peaks mapped to many genes linked to neurodevelopmental and neurological disorders, such as *Bdnf*, *Dscam*, *Lis1*, and *Ube3a*, as well as the neurexins and several neuroligins. Collectively, these data demonstrate that m^{6}A-containing RNAs are involved in a variety of biological pathways that are relevant to cellular signaling and disease.

Because m^{6}A is a physiological target of FTO, we sought to determine whether mRNAs whose levels have previously been shown to be influenced by FTO activity contain m^{6}A. We
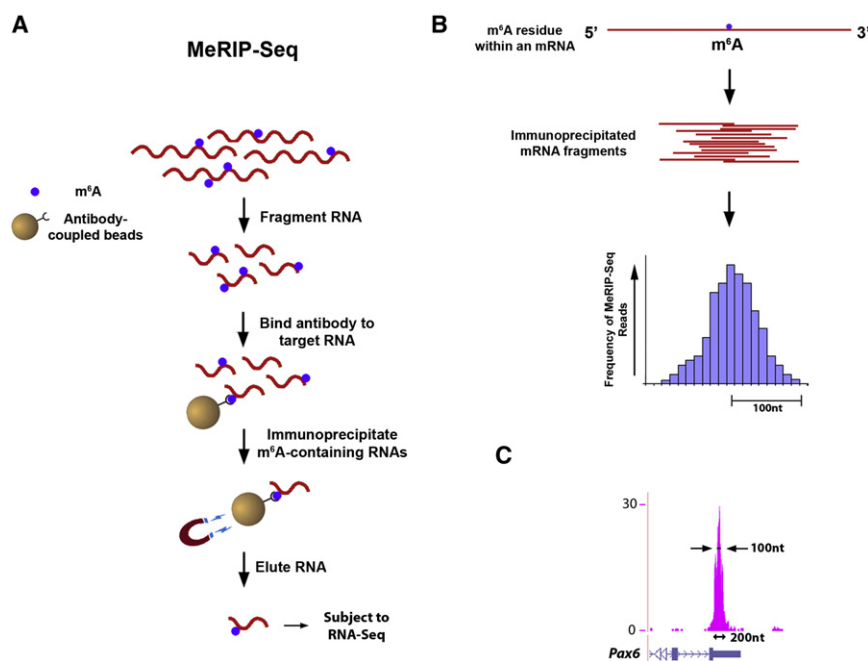
Figure 4. Outline of MeRIP-Seq Protocol and Distribution of Sequencing Reads

(A) Schematic representation of MeRIP-Seq. Total RNA is subjected to RiboMinus treatment to remove rRNA species. RNAs containing m^{6}A are then immunoprecipitated by mixing the RNA with m^{6}A antibody-coupled Dynabeads. m^{6}A-containing RNAs are then eluted from the antibody-coupled beads and subjected to a second round of m^{6}A immunoprecipitation. The resulting RNA pool, which is highly enriched for m^{6}A-containing RNAs, is then subjected to next-generation sequencing.

(B) Schematic of sequencing reads and their alignment to locations in the genome surrounding an m^{6}A site. (Top) An mRNA that contains a single m^{6}A residue along its length. (Middle) Individual 100 nt wide mRNA fragments that are isolated following m^{6}A immunoprecipitation, each of which contains the same m^{6}A residue from the mRNA depicted above. (Bottom) Histogram showing predicted frequency of MeRIP-Seq reads obtained by sequencing individual immunoprecipitated fragments. Read frequency is predicted to increase with closer proximity to the m^{6}A site, forming a "peak" that is roughly 200 nt wide at its base and 100 nt wide at its midpoint.

(C) Sequencing reads from MeRIP-Seq converge over m^{6}A sites. Representative UCSC Genome Browser plot from MeRIP-Seq data, which demonstrates typical read frequency peak formation surrounding a site of m^{6}A (shown here is the 3′ UTR of *Pax6*). Peak height is displayed as reads per base per million mapped reads (BPM).

See also Figures S2 and S3.

examined a list of 77 mRNAs whose levels are either up- or downregulated in the liver, skeletal muscle, or white adipose tissue of mice homozygous for a nonsynonymous FTO point mutation (Church et al., 2009). mRNAs from seven genes that were significantly upregulated in FTO mutants (*Acaca*, *Atf6*, *Bip*, *Gcdh*, *Irs1*, *Perk*, and *Xbp1*) also contain m^{6}A peaks. Intriguingly, some of these genes are involved in important metabolic pathways, raising the possibility that demethylation of the transcripts of these genes may contribute to the mechanism by which FTO regulates metabolism and energy homeostasis.

Diverse Patterns of m^{6}A Localization within Transcripts

We next characterized the pattern of adenosine methylation in mRNAs. mRNAs from many genes (46.0%) exhibit a single m^{6}A peak, consistent with a single m^{6}A site or a cluster of adjacent m^{6}A residues. However, 37.3% contain two m^{6}A peaks, 11.2% contain three peaks, and 5.5% contain four or more peaks. Several genes contain 10 or more m^{6}A peaks, suggesting the existence of multiple m^{6}A residues along their length. Indeed, of the 20 genes that exhibited the largest number of m^{6}A peaks, all had 15 or more m^{6}A peaks along their length (Table S3). Additionally, of the genes that contain more than one m^{6}A peak, 90.1% contain two or more contiguous m^{6}A peaks, suggesting that m^{6}A sites are frequently clustered in adjacent regions along the transcript. Indeed, 32.8% of m^{6}A peaks are part of clusters that contain three or more adjacent m^{6}A peaks, suggesting that m^{6}A clustering is a common feature in methylated transcripts (Figure S6A). We also identified 68 genes that have long (≥ 1 kb) stretches of contiguous m^{6}A peaks (Table S4), which likely indicates the presence of multiple m^{6}A residues throughout these regions.

We next determined which mRNAs contain m^{6}A sites with the highest degree of methylation. To do this, we developed a method of calculating the level of m^{6}A enrichment at individual m^{6}A peaks, which normalized the number of MeRIP sample reads within each peak to the abundance of the individual transcript in which the peak resides (see Extended Experimental Procedures). The genes that contain the most enriched m^{6}A peaks are listed in Table 1. Importantly, because MeRIP-Seq identifies m^{6}A sites at a resolution of 200 nt, there could be multiple individual m^{6}A residues within the area covered by each peak. Therefore, the peaks with the highest levels of local m^{6}A enrichment may represent a single adenosine residue that exhibits a high degree of methylation or multiple adjacent m^{6}A residues with a lower stoichiometry of methylation. In either case, the high levels of methylation observed at these sites likely indicate transcripts that are most influenced by m^{6}A-dependent regulatory processes.

m^{6}A Is Enriched near Stop Codons and in 3′ UTRs of mRNAs

We next examined the distribution of m^{6}A peaks within regions of the transcriptome in our high confidence set. The majority (94.8%) of m^{6}A peaks occur within intragenic regions (Figure 5C). These m^{6}A peaks are abundant in coding sequences (CDS; 50.9%) and untranslated regions (UTRs; 41.9%), with relatively few in intronic regions (2.0%) (Figure 5C). Additionally, m^{6}A peaks are less abundant in the 5′ UTR (7.0% of UTR peaks) than in the 3′ UTR (93.0% of UTR peaks) (Figure 5C). This distribution deviates substantially from the distribution of reads in the non-IP sample, indicating the high degree of enrichment of
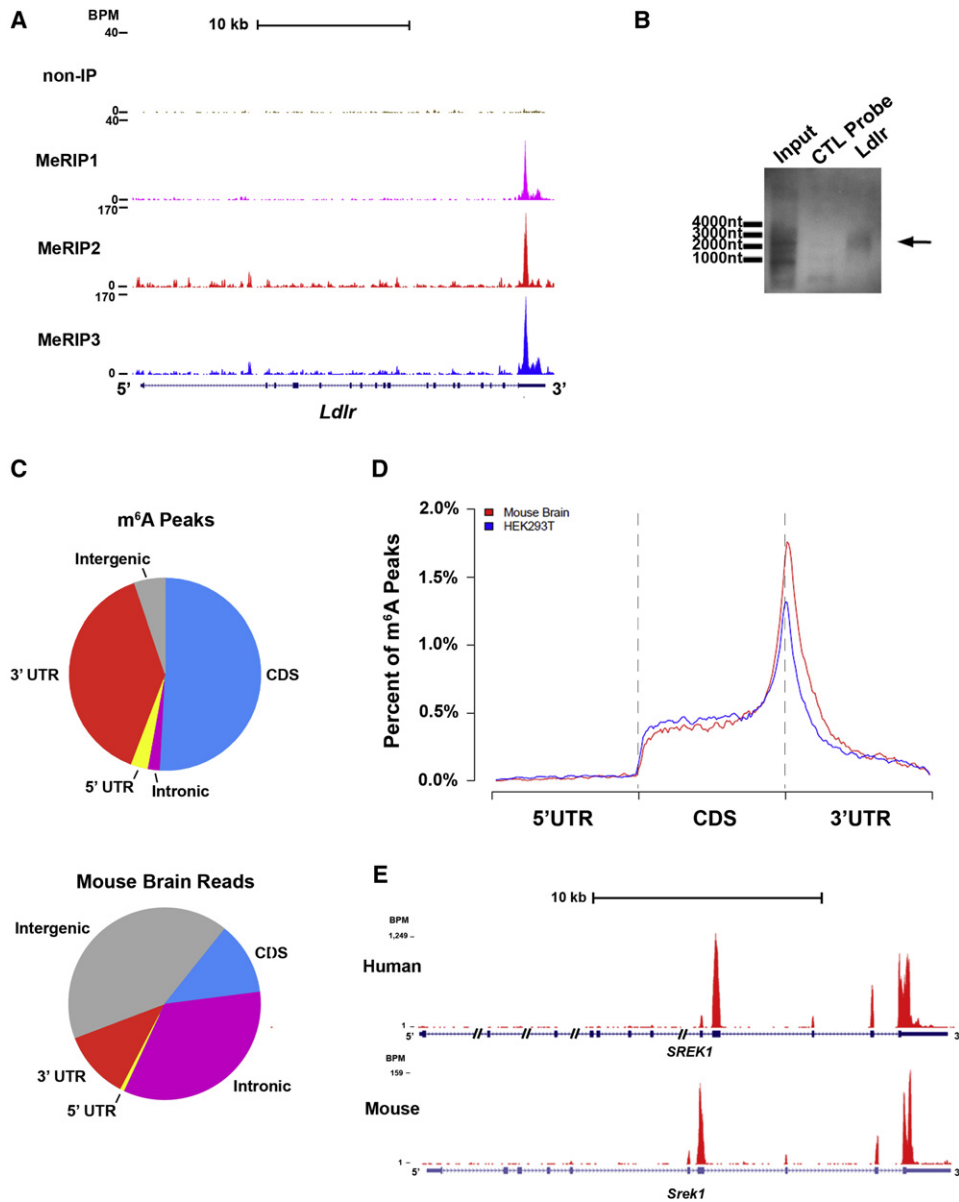
Figure 5. Validation of m⁶A Targets and Characteristics of m⁶A Localization

(A) Different sequencing platforms and antibodies result in similar m⁶A profiles. UCSC Genome Browser tracks displaying read clusters from three MeRIP-Seq replicates (MeRIP1, MeRIP2, and MeRIP3) are shown along the length of the *Ldlr* transcript. The upper-most track (non-IP) represents the non-immunoprecipitated control sample.

(B) Validation of m⁶A-containing mRNA identified with MeRIP-Seq. Hybridization-based RNA pull-down was used to isolate *Ldlr* mRNA from total brain RNA, followed by confirmation of m⁶A presence (arrow) by immunoblot analysis with anti-m⁶A. A control sample using a nonspecific probe of equal size (CTL Probe) was run in parallel. Total mouse brain RNA (Input) is shown as a reference for m⁶A labeling.

(C) Transcriptome-wide distribution of m⁶A peaks. Pie charts showing the percentage of m⁶A peaks (top) and non-IP sample reads (bottom) within distinct RNA sequence types. m⁶A is highly enriched in 3′ UTRs and CDSs compared to the distribution of reads in the non-IP, rRNA-depleted samples.

(D) Distribution of m⁶A peaks across the length of mRNA transcripts. 5′ UTRs, CDSs, and 3′ UTRs of RefSeq mRNAs were individually binned into regions spanning 1% of their total length, and the percentage of m⁶A peaks that fall within each bin was determined. The moving averages of mouse brain peak percentage (red) and HEK293T peak percentage (blue) are shown.

(E) Highly similar m⁶A peak distribution is observed within many human and mouse transcripts. UCSC Genome Browser plots showing MeRIP-Seq read clusters in the representative transcript *SREK1*. MeRIP-Seq reads cluster at the same distinct regions of *SREK1* in both HEK293T cell RNA (top) and mouse brain RNA (bottom).

See also Figures S4–S7 and Tables S1–S6.

Table 1. Genes Encoding Transcripts with the Highest Degree of m⁶A Enrichment

Chr	Peak Start	Peak End	RefSeq Accession	Gene Symbol	Enrichment Score
chr6	58856032	58856214	NM_021432	Nap1l5	3.859
chr3	30717625	30717825	NM_027016	Sec62	3.693
chr3	88566067	88566234	NM_018804	Syt11	3.452
chr6	58855850	58856032	NM_021432	Nap1l5	3.327
chr19	5801367	5801534	NR_002847	Malat1	3.322
chr12	110898950	110899150	NR_028261	Rian	3.222
chr10	34018834	34018993	NM_030203	Tspyl4	3.162
chr17	6138575	6138775	NM_054040	Tulp4	2.984
chr2	34631357	34631514	NM_001163434	Hspa5	2.935
chr2	102630175	102630350	NM_001077514	Slc1a2	2.933
chr11	7072225	7072425	NM_009622	Adcy1	2.865
chr2	158211200	158211350	NM_175692	Snhg11	2.788
chr15	37326800	37327000	NM_134094	Ncald	2.685
chr2	102629600	102629788	NM_001077514	Slc1a2	2.672
chr15	37327000	37327200	NM_134094	Ncald	2.656
chr10	80644950	80645125	NM_007907	Eef2	2.451
chr2	102629788	102629975	NM_001077514	Slc1a2	2.392
chr11	59251613	59251750	NM_144521	Snap47	2.306
chr15	74581075	74581267	NM_011838	Lynx1	2.258
chr2	158211050	158211200	NM_175692	Snhg11	2.102

Shown are the top 20 genes that contain m⁶A peaks with the highest levels of enrichment.

m⁶A peaks in the CDS and UTRs (Figure 5C). Although a low percentage of m⁶A peaks was observed in intronic regions, because our samples were not enriched for unspliced pre-mRNAs, it is possible that additional methylated intronic sequences exist.

We next sought to determine whether m⁶A peaks are preferentially found in certain portions of transcripts. To do this, we assigned each m⁶A peak to either a 5′ UTR, CDS, or 3′ UTR category and assigned it to 1 of 100 bins based on its location along the 5′ UTR, CDS, or 3′ UTR. These data show that m⁶A occurs at low levels in the 5′ UTR and in the 5′ end of the CDS. In the CDS, the percentage of m⁶A peaks increases steadily along transcript length and is, on average, 5- to 6-fold higher at the end of the CDS than at the beginning (Figure 5D). In the 3′ UTR, the peaks are enriched near the stop codon and decrease in abundance along the length of the 3′ UTR. Indeed, 61% of m⁶A peaks are in the first quarter of the 3′ UTR, and a quarter of all m⁶A peaks across the entire transcriptome are found within the first 26% of the 3′ UTR (Figure 5D). Mapping the number of m⁶A peaks 1 kb up- and downstream of CDS end sites further demonstrated the high levels of methylation in the vicinity of the stop codon (Figures S7A and S7B). Collectively, these data indicate that m⁶A peaks are highly clustered in the vicinity of the stop codon in mRNAs.

m⁶A Occurs in Highly Conserved Regions within Unique Sequence Motifs

We next asked whether m⁶A sites are conserved across species. We compared PhyloP scores across 30 vertebrates (Pollard et al., 2010) of m⁶A peak regions to those of random regions of the same size in gene exons. We found that the distribution of conservation scores of the m⁶A peaks was significantly different from that of the random regions (p ≤ 2.2 × 10⁻¹⁶, Kolmogorov-Smirnov [K-S] test; Figure 6A) and that m⁶A peaks' median conservation score (0.578) was much higher than that of the random regions (0.023). The fact that m⁶A frequently occurs in evolutionarily conserved sequences suggests that m⁶A-containing regions are maintained through selection pressure.

Because the tools for transcriptome-wide localization of m⁶A sites have until now been unavailable, only a few studies to date have examined the sequence contexts of m⁶A formation (Canaani et al., 1979; Dimock and Stoltzfus, 1977; Wei et al., 1976). Using methods such as RNase T1 fingerprinting of radiolabeled RNA followed by separation by thin-layer chromatography, these studies reported that m⁶A exists within two unique sequence contexts: G<u>A</u>C and A<u>A</u>C (underlined adenosines indicate m⁶A). Subsequently, an extended m⁶A consensus sequence was identified: PuPu<u>A</u>CX (Pu = purine; X = A, C, or U). However, because the methods used in these studies are not practical for use in a high-throughput manner, it is unclear whether these motifs are relevant to the transcriptome-wide m⁶A sites identified by MeRIP-Seq.

We therefore sought to identify sequence motifs that are enriched within m⁶A peaks. To do this, we used FIRE, a sensitive and unbiased tool for discovering RNA regulatory elements (Elemento et al., 2007). Remarkably, FIRE independently identified the GAC and AAC motif, G[AG]ACU, and related variants ([AC]GAC[GU], GGAC, [AU][CG]G[AG]AC, and UGAC) as being
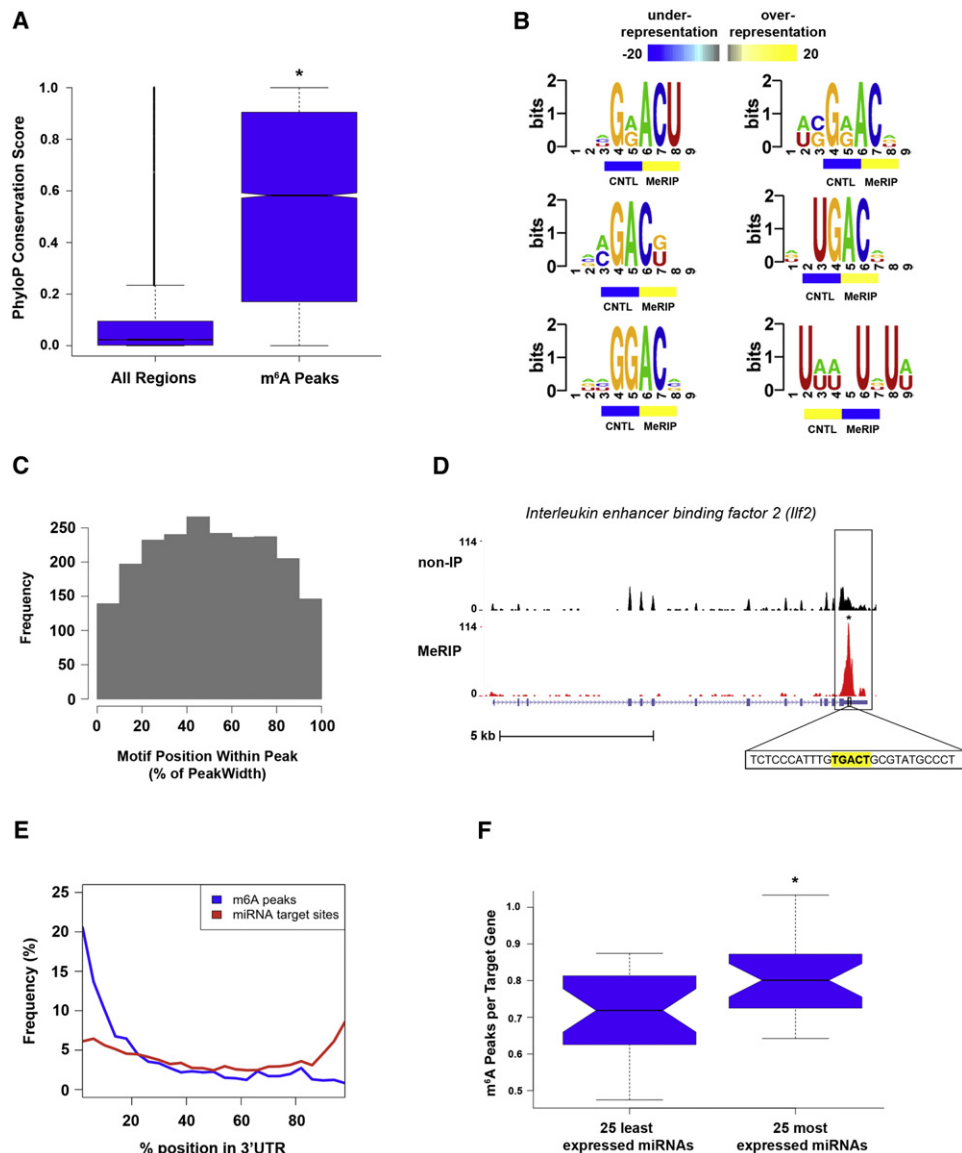
Figure 6. MeRIP-Seq Reveals Features of m⁶A in mRNA

(A) Phylogenetic conservation of m^{6}A peaks. PhyloP scores of m^{6}A peak regions were compared to those of randomly shuffled regions throughout gene exons. There was a significantly higher median conservation score (K-S test, $*p \leq 2.2 \times 10^{-16}$) in m^{6}A peaks (0.578) than in the random regions (0.023).

(B) Sequence motifs identified within m^{6}A peaks. The motif G[AG]ACU and variants thereof ([AC]GAC[GU], GGAC, [AU][CG]G[AG]AC, and UGAC) were highly enriched in m^{6}A peaks. Additionally, one U-rich motif (lower-right) was identified as being significantly underrepresented within m^{6}A peaks. Color bars under each motif indicate the degree of underrepresentation (blue) or overrepresentation (yellow) within regions of m^{6}A peaks in the non-IP control sample (CNTL) and the MeRIP sample (MeRIP).

(C) m^{6}A motif sequences frequently lie near the center of m^{6}A peaks. Shown is a plot of the cumulative distribution of m^{6}A motif positions within m^{6}A peaks containing a single motif. Motifs cluster in the center of peaks, suggesting that the methylated adenosines in these motifs account for the m^{6}A peaks identified in MeRIP-Seq.

(D) Example of a m^{6}A motif sequence near the center of a peak. UCSC Genome Browser plot containing tracks for MeRIP-Seq reads (red) and non-IP control reads (black) at the *Ilf2* locus. The m^{6}A peak within the *Ilf2* 3′ UTR contains a single m^{6}A motif identified in (B). The sequence of this motif (highlighted in yellow) is located at the center of the m^{6}A peak.

(E) Distribution of m^{6}A peaks and miRNA target sites within 3′ UTRs. The frequency of m^{6}A peaks (blue) and miRNA target sites (red) along the length of 3′ UTRs is shown.

(F) Association between 3′ UTR methylation and miRNA abundance. The 25 most abundant miRNAs in brain have a significantly greater percentage of m^{6}A peaks within their target mRNA 3′ UTRs than do the 25 most weakly expressed brain miRNAs ($*p < 0.05$, Wilcoxon test).

The error bars in (A) and (F) indicate the highest and lowest values, and the box boundaries denote the first quartile, median, and third quartile.

See also Figures S3, S6, and S7.

highly enriched in m⁶A peaks (Figure 6B). For example, the G[AG]ACU motif occurs in 42% of all m⁶A mRNA peaks and in a much lower fraction (21%) of non-m⁶A control peaks from the same mRNAs (p < 1.0 × 10^{-124}, chi-square test). Altogether, we found that >90% of all m⁶A peaks contain at least one of the motifs identified by FIRE.

We next examined the position of the motifs within m⁶A peaks. Nearly 30% of m⁶A peaks have only one motif (Figure S6B), indicating that these peaks are likely to contain only a single methylated residue. Motifs are also preferentially found in the center of m⁶A peaks (Figures 6C and 6D), suggesting that these peaks derive from a centrally located methylated adenosine residue. Of note, other RNA regulatory elements, such as AU-rich elements, poly(A) signals, or binding sites for known RNA-binding proteins, were not identified by FIRE, suggesting that m⁶A is unlikely to primarily function by modifying these known regulatory elements.

Relationship between m⁶A Sites and Polyadenylation Signals in 3′ UTRs

FIRE did not identify an enrichment of poly(A) signals (PASs), which are involved in 3′ UTR end processing, in m⁶A peaks. However, PASs exhibit considerable sequence heterogeneity beyond the canonical AAUAAA consensus (Tian et al., 2005). This sequence heterogeneity might allow these PASs to evade detection by FIRE despite being enriched in m⁶A peaks. Therefore, we sought to further investigate whether m⁶A peaks within 3′ UTRs are enriched at PASs. We obtained a high-confidence list (Brockman et al., 2005) of poly(A) cleavage sites (the site downstream of a PAS where the mRNA is actually cleaved and polyadenylated) for the mRNAs that contain m⁶A peaks within their 3′ UTRs. We then examined whether m⁶A peaks were enriched near these sites by determining the number of 3′ UTR m⁶A peaks that fell within 50 nt upstream of each cleavage site. Because a PAS is located ~10–30 nt upstream of an actual mRNA cleavage site (reviewed in Proudfoot, 1991), these 50 nt long regions are expected to contain the PAS. Of the 6,288 m⁶A peaks found within 3′ UTRs, 1,042 (16.6%) overlapped with the 50 nt long regions upstream of poly(A) cleavage sites, compared to 1,070 (17.0%) control peaks, which were generated from random nonoverlapping regions of the same 3′ UTRs. Thus, these data suggest that m⁶A does not have a significant association with known PASs (p = 0.39; chi-square test).

m⁶A Is Not Enriched at Splice Junctions

Prior studies that used nonspecific methylation inhibitors to explore possible functions for m⁶A revealed impaired splicing in a small number of RNAs (Carroll et al., 1990; Stoltzfus and Dane, 1982). We therefore asked whether the localization of m⁶A peaks is compatible with a role for influencing the binding of splicing factors. However, only 80 splice junctions were found in regions contiguous with m⁶A peaks, significantly fewer than the overlap seen with a set of randomly generated peaks (9,531; p = 0.0; chi-square test). Thus, unlike CLIP-Seq tag clusters from RNA-binding proteins that influence splicing (Licatalosi et al., 2008), m⁶A peaks did not significantly coincide with exon-exon junctions, suggesting that m⁶A is unlikely

to primarily function to directly influence the binding of splicing factors.

Relationship between m⁶A and MicroRNA-Binding Sites within 3′ UTRs

The strong enrichment of m⁶A peaks in 3′ UTRs prompted us to investigate whether m⁶A peaks are found near microRNA (miRNA)-binding sites, which are also frequently observed within 3′ UTRs. We found that 67% of 3′ UTRs that contain m⁶A peaks also contain at least one TargetScan-predicted miRNA-binding site. Because ~30% of genes have miRNA-binding sites in their 3′ UTRs (Lewis et al., 2005), this is a significantly greater association than what would be expected by chance alone. Intriguingly, we also found that, in 3′ UTRs with both m⁶A peaks and miRNA-binding sites, the m⁶A peaks precede miRNA-binding sites 62% of the time. Moreover, we found that the overall distribution of m⁶A peaks and miRNA-binding sites within 3′ UTRs is anti-correlated; whereas m⁶A peaks are most abundant near the stop codon and generally decrease in frequency along 3′ UTR length, miRNA target sites are more enriched near the 3′ end of 3′ UTRs (Figure 6E). The reason for this inverse localization pattern is unknown, though it could indicate that a certain spatial separation is necessary for m⁶A to influence the function of a downstream-bound miRNA or vice versa.

We next sought to determine whether miRNA-targeted transcripts in the brain are more likely to contain m⁶A. To test this, we used TargetScan to identify the target transcripts of the 25 most highly expressed and 25 least highly expressed miRNAs within the brain. Intriguingly, we observed that the most highly expressed miRNAs have a significantly greater percentage of target transcripts that contain m⁶A (p < 0.05, Wilcoxon test; Figure 6F). These data suggest that miRNA levels may control methylation of their target transcripts.

Prominent Features of m⁶A Distribution Are Conserved in the Human Transcriptome

We next asked whether the enrichment of m⁶A in the 3′ UTR is also observed in other species. We therefore profiled m⁶A in HEK293T cells, a human cell line with high levels of adenosine methylation (Figure 3B). We generated a high-confidence list of m⁶A peaks using three MeRIP-Seq biological replicates and confirmed by both m⁶A antibodies. We found that the distribution of m⁶A peaks in HEK293T cells closely mirrored the distribution in mouse brain, with 31% and 53% of m⁶A peaks falling within the 3′ UTR and the CDS, respectively (Figures 5D and S7D). As with the pattern of m⁶A distribution in the mouse brain transcriptome, HEK293T m⁶A peaks were predominantly localized near stop codons (Figures 5D and S7C).

In total, we identified 18,756 peaks in RNAs encoded by 5,768 genes in HEK293T cells (Table S6A). Additionally, we found that transcripts from 2,145 and 3,259 genes were methylated only in the mouse brain and HEK293T data sets, respectively, and that transcripts from 2,509 genes were methylated in both data sets (Table S6B). Interestingly, among the transcripts methylated in both tissues, m⁶A peaks were often localized to the same distinct regions of both orthologs (Figure 5E). Collectively, these data indicate that m⁶A peaks are enriched near the stop codon in

human transcripts and that many sites of methylation are conserved in mouse and human transcripts.

DISCUSSION

Unlike DNA, which undergoes cytosine methylation and hydroxymethylation, dynamic internal modifications of mRNA other than RNA editing have not been established. Recent evidence that the obesity risk gene, *FTO*, encodes a physiologic m^6A demethylase suggests that m^6A has central roles in cellular function. Here, we use MeRIP-Seq to provide the first transcriptome-wide characterization of m^6A. We show that m^6A is a reversible and widespread modification that is primarily located in evolutionarily conserved regions and is particularly enriched near the stop codon. We also find that many features of m^6A localization are conserved between the human and mouse transcriptomes, and we uncover a previously unidentified link between m^6A and miRNA signaling. Collectively, these studies reveal that m^6A is a widespread and dynamically regulated base modification in mRNA, and they identify mRNAs that are most likely to be influenced by signaling pathways that influence m^6A levels.

One of the most striking features of m^6A localization is its prevalence within 3′ UTRs. The 3′ UTR is an important region for RNA regulation, as it can influence RNA stability, subcellular localization, and translation regulation. Several of these events are regulated by RNA-binding proteins (RBPs) that bind to *cis*-acting structural motifs or consensus sequences within the 3′ UTR and act to coordinate RNA processing. Conceivably, m^6A may influence the affinity of specific RBPs for their target mRNAs, analogous to the recruitment of methyl-CpG-binding protein 2 (MeCP2) to methylated cytosine residues in DNA (Lewis et al., 1992). Given the abundance of m^6A throughout the transcriptome and its widespread localization, such a role for m^6A would be likely to have important consequences for the regulation of numerous mRNAs.

Our profiling of m^6A in HEK293T cells revealed thousands of transcripts that are also methylated in the mouse brain. In many cases, the patterns of m^6A localization within these transcripts are nearly identical, suggesting that some RNAs possess highly conserved methylation profiles. However, we also uncovered many transcripts that exhibit distinct cell-type-specific methylation patterns, demonstrating that m^6A is also capable of being differentially regulated within unique cellular environments.

Our finding that a large proportion of 3′ UTRs that contain m^6A peaks also contain miRNA binding sites is highly suggestive of an association between m^6A and miRNA function. Additionally, our analysis indicated an inverse localization of m^6A peaks and miRNA-binding sites within 3′ UTRs, with m^6A sites typically preceding, but not overlapping, the miRNA sites in the 3′ UTRs. Although miRNAs can inhibit their target mRNAs by promoting either transcript degradation or translational repression (Guo et al., 2010; Hendrickson et al., 2009), the factors that determine which fate predominates are not well understood. Conceivably, the proximity of m^6A to a miRNA-binding site could influence the mechanism of miRNA-mediated transcript inhibition. Additionally, it is possible that miRNA binding influences m^6A levels within 3′ UTRs. Indeed, our finding that abundant miRNAs are more significantly enriched in m^6A peaks than weakly expressed miRNAs raises the possibility that miRNAs regulate methylation status.

A surprising result of these studies is the finding that m^6A is highly enriched near stop codons. This recurrent localization within transcripts suggests that adenosine methylation in the vicinity of the stop codon may be of functional importance. Interestingly, the consensus for adenosine methylation is relatively short, and sequences that match the consensus are found throughout the transcriptome. However, despite the frequency of m^6A consensus sites, methylation occurs primarily near stop codons. It will be important to determine how this specificity is achieved and whether cellular mechanisms that involve recognition of the stop codon or the beginning of the 3′ UTR are involved in providing specificity to adenosine methylation.

The finding that FTO demethylates m^6A suggests that misregulation of pathways controlled by adenosine methylation ultimately affect physiologic processes in humans. Although m^6A is found in many classes of RNA, it is intriguing to speculate that FTO mutations mediate their effects by affected m^6A in mRNA. Indeed, our finding that FTO can demethylate diverse mRNAs is consistent with this model. Direct characterization of m^6A profiles in patients with *FTO* mutations will be useful to establish the mechanisms by which this mutation leads to disease.

In summary, our study demonstrates that m^6A is a widespread modification found in a large fraction of cellular mRNA. The pervasive nature of this epitranscriptomic modification suggests that adenosine methylation has important roles in RNA biology. Much in the way that cytosine methylation and hydroxymethylation in DNA are important epigenetic regulators of the genome, our data demonstrate that adenosine methylation in RNA is a reversible modification throughout the transcriptome that is likely to influence a wide variety of biological pathways and physiological processes.

EXPERIMENTAL PROCEDURES

MeRIP-Seq

Total mouse brain RNA was subjected to RiboMinus treatment to reduce rRNA content as per the manufacturer's instructions (Invitrogen). RNA was then fragmented to 100 nt sized fragments using Illumina Fragmentation Buffer according to the manufacturer's instructions and was subjected to two rounds of m^6A immunoprecipitation. Sequencing libraries were prepared using the Illumina protocol for mRNA samples, and sequencing was performed on an Illumina GAII× or an Illumina HiSeq2000 as indicated. Genomic alignment (mm9 or hg19 from UCSC genome browser) was done using the Burrows-Wheeler Aligner (BWA) (Li and Durbin, 2010) at default settings, or using TopHat (see Extended Experimental Procedures). We analyzed only those reads that (1) uniquely mapped to the genome and (2) had a Phred quality score ≥20.

Additional methods are detailed in the Extended Experimental Procedures.

ACCESSION NUMBERS

MeRIP-Seq data have been deposited in the GEO database under accession number GSE29714.

SUPPLEMENTAL INFORMATION

Supplemental Information includes Extended Experimental Procedures, seven figures, and six tables and can be found with this article online at doi:10.1016/j.cell.2012.05.003.

REFERENCES

Beemon, K., and Keith, J. (1977). Localization of N6-methyladenosine in the Rous sarcoma virus genome. J. Mol. Biol. *113*, 165–179.

Bodi, Z., Button, J.D., Grierson, D., and Fray, R.G. (2010). Yeast targets for mRNA methylation. Nucleic Acids Res. *38*, 5327–5335.

Bringmann, P., and Lührmann, R. (1987). Antibodies specific for N6-methyladenosine react with intact snRNPs U2 and U4/U6. FEBS Lett. *213*, 309–315.

Brockman, J.M., Singh, P., Liu, D., Quinlan, S., Salisbury, J., and Graber, J.H. (2005). PACdb: PolyA Cleavage Site and 3′-UTR Database. Bioinformatics *21*, 3691–3693.

Cabili, M.N., Trapnell, C., Goff, L., Koziol, M., Tazon-Vega, B., Regev, A., and Rinn, J.L. (2011). Integrative annotation of human large intergenic noncoding RNAs reveals global properties and specific subclasses. Genes Dev. *25*, 1915–1927.

Canaani, D., Kahana, C., Lavi, S., and Groner, Y. (1979). Identification and mapping of N6-methyladenosine containing sequences in simian virus 40 RNA. Nucleic Acids Res. *6*, 2879–2899.

Carroll, S.M., Narayan, P., and Rottman, F.M. (1990). N6-methyladenosine residues in an intron-specific region of prolactin pre-mRNA. Mol. Cell. Biol. *10*, 4456–4465.

Church, C., Lee, S., Bagg, E.A., McTaggart, J.S., Deacon, R., Gerken, T., Lee, A., Moir, L., Mecinović, J., Quwailid, M.M., et al. (2009). A mouse model for the metabolic effects of the human fat mass and obesity associated FTO gene. PLoS Genet. *5*, e1000599.

Church, C., Moir, L., McMurray, F., Girard, C., Banks, G.T., Teboul, L., Wells, S., Brüning, J.C., Nolan, P.M., Ashcroft, F.M., and Cox, R.D. (2010). Overexpression of Fto leads to increased food intake and results in obesity. Nat. Genet. *42*, 1086–1092.

Csepany, T., Lin, A., Baldick, C.J., Jr., and Beemon, K. (1990). Sequence specificity of mRNA N6-adenosine methyltransferase. J. Biol. Chem. *265*, 20117–20122.

Desrosiers, R., Friderici, K., and Rottman, F. (1974). Identification of methylated nucleosides in messenger RNA from Novikoff hepatoma cells. Proc. Natl. Acad. Sci. USA *71*, 3971–3975.

Dimock, K., and Stoltzfus, C.M. (1977). Sequence specificity of internal methylation in B77 avian sarcoma virus RNA subunits. Biochemistry *16*, 471–478.

Dubin, D.T., and Taylor, R.H. (1975). The methylation state of poly A-containing messenger RNA from cultured hamster cells. Nucleic Acids Res. *2*, 1653–1668.

Elemento, O., Slonim, N., and Tavazoie, S. (2007). A universal framework for regulatory element discovery across all genomes and data types. Mol. Cell *28*, 337–350.

Falnes, P.O., Klungland, A., and Alseth, I. (2007). Repair of methyl lesions in DNA and RNA by oxidative demethylation. Neuroscience *145*, 1222–1232.

Fawcett, K.A., and Barroso, I. (2010). The genetics of obesity: FTO leads the way. Trends Genet. *26*, 266–274.

Fischer, J., Koch, L., Emmerling, C., Vierkotten, J., Peters, T., Brüning, J.C., and Rüther, U. (2009). Inactivation of the Fto gene protects from obesity. Nature *458*, 894–898.

Gerken, T., Girard, C.A., Tung, Y.C., Webby, C.J., Saudek, V., Hewitson, K.S., Yeo, G.S., McDonough, M.A., Cunliffe, S., McNeill, L.A., et al. (2007). The obesity-associated FTO gene encodes a 2-oxoglutarate-dependent nucleic acid demethylase. Science *318*, 1469–1472.

Guo, H., Ingolia, N.T., Weissman, J.S., and Bartel, D.P. (2010). Mammalian microRNAs predominantly act to decrease target mRNA levels. Nature *466*, 835–840.

Hendrickson, D.G., Hogan, D.J., McCullough, H.L., Myers, J.W., Herschlag, D., Ferrell, J.E., and Brown, P.O. (2009). Concordant regulation of translation and mRNA abundance for hundreds of targets of a human microRNA. PLoS Biol. *7*, e1000238.

Horowitz, S., Horowitz, A., Nilsen, T.W., Munns, T.W., and Rottman, F.M. (1984). Mapping of N6-methyladenosine residues in bovine prolactin mRNA. Proc. Natl. Acad. Sci. USA *81*, 5667–5671.

Iwanami, Y., and Brown, G.M. (1968). Methylated bases of ribosomal ribonucleic acid from HeLa cells. Arch. Biochem. Biophys. *126*, 8–15.

Jia, G., Yang, C.G., Yang, S., Jian, X., Yi, C., Zhou, Z., and He, C. (2008). Oxidative demethylation of 3-methylthymine and 3-methyluracil in single-stranded DNA and RNA by mouse and human FTO. FEBS Lett. *582*, 3313–3319.

Jia, G., Fu, Y., Zhao, X., Dai, Q., Zheng, G., Yang, Y., Yi, C., Lindahl, T., Pan, T., Yang, Y.G., et al. (2011). N6-methyladenosine in nuclear RNA is a major substrate of the obesity-associated FTO. Nat. Chem. Biol. *7*, 885–887.

Klagsbrun, M. (1973). An evolutionary study of the methylation of transfer and ribosomal ribonucleic acid in prokaryote and eukaryote organisms. J. Biol. Chem. *248*, 2612–2620.

Kong, H., Lin, L.F., Porter, N., Stickel, S., Byrd, D., Posfai, J., and Roberts, R.J. (2000). Functional analysis of putative restriction-modification system genes in the Helicobacter pylori J99 genome. Nucleic Acids Res. *28*, 3216–3223.

Lewis, J.D., Meehan, R.R., Henzel, W.J., Maurer-Fogy, I., Jeppesen, P., Klein, F., and Bird, A. (1992). Purification, sequence, and cellular localization of a novel chromosomal protein that binds to methylated DNA. Cell *69*, 905–914.

Lewis, B.P., Burge, C.B., and Bartel, D.P. (2005). Conserved seed pairing, often flanked by adenosines, indicates that thousands of human genes are microRNA targets. Cell *120*, 15–20.

Li, H., and Durbin, R. (2010). Fast and accurate long-read alignment with Burrows-Wheeler transform. Bioinformatics *26*, 589–595.

Licatalosi, D.D., Mele, A., Fak, J.J., Ule, J., Kayikci, M., Chi, S.W., Clark, T.A., Schweitzer, A.C., Blume, J.E., Wang, X., et al. (2008). HITS-CLIP yields genome-wide insights into brain alternative RNA processing. Nature *456*, 464–469.

Munns, T.W., Liszewski, M.K., and Sims, H.F. (1977). Characterization of antibodies specific for N6-methyladenosine and for 7-methylguanosine. Biochemistry *16*, 2163–2168.

Narayan, P., and Rottman, F.M. (1988). An in vitro system for accurate methylation of internal adenosine residues in messenger RNA. Science *242*, 1159–1162.

Pang, K.C., Stephen, S., Engström, P.G., Tajul-Arifin, K., Chen, W., Wahlestedt, C., Lenhard, B., Hayashizaki, Y., and Mattick, J.S. (2005). RNAdb—a comprehensive mammalian noncoding RNA database. Nucleic Acids Res. *33* (*Database issue*), D125–D130.

Perry, R.P., Kelley, D.E., Friderici, K., and Rottman, F. (1975). The methylated constituents of L cell messenger RNA: evidence for an unusual cluster at the 5′ terminus. Cell *4*, 387–394.

Pollard, K.S., Hubisz, M.J., Rosenbloom, K.R., and Siepel, A. (2010). Detection of nonneutral substitution rates on mammalian phylogenies. Genome Res. *20*, 110–121.

Proudfoot, N. (1991). Poly(A) signals. Cell *64*, 671–674.

Saneyoshi, M., Harada, F., and Nishimura, S. (1969). Isolation and characterization of N6-methyladenosine from Escherichia coli valine transfer RNA. Biochim. Biophys. Acta *190*, 264–273.

Stoltzfus, C.M., and Dane, R.W. (1982). Accumulation of spliced avian retrovirus mRNA is inhibited in S-adenosylmethionine-depleted chicken embryo fibroblasts. J. Virol. *42*, 918–931.

Tian, B., Hu, J., Zhang, H., and Lutz, C.S. (2005). A large-scale analysis of mRNA polyadenylation of human and mouse genes. Nucleic Acids Res. *33*, 201–212.

Wei, C.M., Gershowitz, A., and Moss, B. (1975). Methylated nucleotides block 5′ terminus of HeLa cell messenger RNA. Cell *4*, 379–386.

Wei, C.M., Gershowitz, A., and Moss, B. (1976). 5′-Terminal and internal methylated nucleotide sequences in HeLa cell mRNA. Biochemistry *15*, 397–401.